Zhou Hua Jiang*, Jia Yu, Fu Bin Liu, Xu Chen and Xin Geng

Application of Mathematical Models for Different Electroslag Remelting Processes

DOI 10.1515/htmp-2016-0146
Received July 5, 2016; accepted January 7, 2017

Abstract: The electroslag remelting (ESR) process has been effectively applied to produce high grade special steels and super alloys based on the controllable solidification and chemical refining process. Due to the difficulties of precise measurements in a high temperature environment and the excessive expenses, mathematical models have been more and more attractive in terms of investigating the transport phenomena in ESR process. In this paper, the numerical models for different ESR processes made by our lab in last decade have been introduced. The first topic deals with traditional ESR process predicting the relationship between operating parameters and metallurgical parameters of interest. The second topic is concerning the new ESR technology process including ESR with current-conductive mould (CCM), ESR hollow ingot technology, electroslag casting with liquid metal(ESC LM), and so on. Finally, the numerical simulation of solidification microstructure with multi-scale model is presented, which reveals the formation mechanism of microstructure.

Keywords: electroslag remelting, mathematical models, transport processes, solidification structure

Introduction

Electroslag remelting is widely applied in manufacture of high grade special steels and super alloys with the character of high cleanliness, homogenous composition and compact structure which have been used in many industrial fields such as aerospace, aviation, energy, ship building, electronics, petrochemical industry, heavy machinery, transportation and so on. [1–3]. Figure 1 shows a schematic of the ESR process. The passage of an AC or DC current from the electrode to the water-cooled base plate results in Joule heating within the highly resistive calcium fluoride-based slag, which is enough to melt the electrode in the form of metallic drops. The drops travel through the slag and gather in the water-cooled mold where they solidify. Fine solidification structure with low macro/micro segregation is a main advantage of ESR.

Low productivity, high power consumption, pollution of the environment due to CaF_2 and macro/micro segregation in large-scale ESR ingots with high alloy are the main shortcomings of traditional ESR process, which could be improved by optimizing traditional ESR process and developing new ESR processes. Given the high costs and the difficulties of precise measurements in a high temperature environment [4], it is impracticable to study the effects of parameters on the final ingot quality by trial and error. Hence, the alternative of using mathematical models to investigate the ESR process has gained more and more attention. Over the past decades, many mathematical models have been developed to study the mass, momentum and heat transfer phenomena in ESR process.

Sun and Pridgeon [5] obtained the temperature distribution of the ingot using a transient heat transfer model excluding the fluid flow in molten metal pool. Hence, the model has some limitations in predicting pool profile and could only be as a reference.

Carvajal and Gerger [6] improved the Sun and Pridgeon's model with a parabolic shaped profile of temperature imposed on the slag/pool interface, and assumed the heat transfer coefficient at the ingot/mould interface varying with the axial position. The model acquired satisfactory results compared with measured data, which was a significant progress.

Dilawari and Szekely [7, 8] originally developed a mathematical model to represent the electromagnetic field and fluid flow in ESR system, and compared the industrial scale and laboratory scale ESR process simultaneously. However, the pool profile was assumed in advance due to the absence of heat transfer.

Choudhary et al. further developed the Dilawari's model [9]. The pool profile was obtained by solving energy conservation equation with the assumption that the effect of convection in metal pool on heat transfer was taken into account by the effective thermal conductivity. The predicted pool profile was in agreement with

***Corresponding author: Zhou Hua Jiang,** School of Metallurgy, Northeastern University, Shenyang 110819, China,
E-mail: jiangzh@smm.neu.edu.cn
Jia Yu, Fu Bin Liu, Xu Chen, Xin Geng, School of Metallurgy, Northeastern University, Shenyang 110819, China

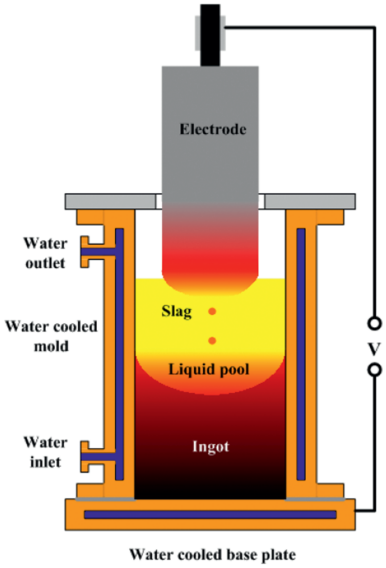

Figure 1: Schematic sketch of electroslag remelting.

the measured result. Besides, the relationship between the key metallurgical parameters of interest and operation parameters was also studied. In order to validate model the flow of mercury in a horizontal trough through which a current was being passed via two electrodes was observed [10]. The velocity field obtained by the photographic technique agreed well with the computed results.

Ferng et al. also developed an integrated numerical model to compute the electromagnetic field, flow and heat characteristics inside ESR units where the pool profile was determined by an iterative process. Above all, the flow and turbulent mixing in liquid pool was firstly calculated, which was not considered in previous papers. In addition, the authors compared the effects of power supply type on the flow pattern and found that the calculated velocity distribution in slag was similar for both AC and DC power, but a secondary loop zone appeared at the slag/metal interface when AC power was applied [11].

Kharicha et al. predicted the heat flux from the melting interface into the electrode by solving a 1D Stefan problem [12, 13], and found that the coupling between the Joule heat release and melt rate was extremely unstable. Hence, the model was modified based on the dynamic mesh technique, the feeding rate of electrode was adjusted with the immersion depth. Besides, the effects of electric conductivity and thermal conductivity of slag on the melt rate and shape of electrode tip were investigated.

Fezi and Yanke et al. developed a continuum mixture model for conservation equations in both slag and metal coupled with a multicomponent alloy solidification model to study the macrosegregation in production of alloy 625. The melt rate was calculated with a 1D heat conduction model, and the growth of ingot was taken into account by a moving mesh technique. They concluded that processing ingot with a low current and small ingot size contributes to reduce the macrosegregation. Furthermore, they applied a modified volume of fluid to investigate the formation and melting of slag skin, and indicated that the variable slag skin thickness affects melt rate and sump depth [14, 15].

Wang et al. established a 3D transient mathematical model to study the coupled physical fields in electroslag remelting process. The electromagnetic field varied dynamically with the phase distribution was investigated using the MHD module, and showed that the Lorentz force tended to block the motion of the metallic droplet. Besides, a thermodynamic and kinetics module was contained in the numerical model to study the desulfurization behavior in ESR process, the results indicated that the maximum calculated removal ratio could reach up to 71% [16, 17].

Some other researches are summarized as following: Jiang et al. studied the distribution of electric potential and Joule heat in ESR system [18, 19]. Wei et al. discussed the influence of slag component and electrical parameters on the ESR process [20, 21]. Liang et al. considered the effects of applied frequency of AC on the current density distribution and Lorentz force using the MeltFlow [22]. Weber et al. developed a comprehensive model validated by a comparison between the experimental and calculated pool profile, which could be used to predict the behavior of an ESR operation [23]. Dong et al. investigated the electroslag casting solid ingot with liquid metal and multi-electrodes electroslag remelting process using mathematical model [24, 25].

This paper aims to introduce our numerical simulation results in traditional and new electroslag remelting technology, which are given through several examples as below. Besides, the outlooks for numerical simulation of ESR process have been proposed.

Mathematical model and validation for electroslag remelting process

Mathematical model

The numerical simulation of electroslag remelting involves with the coupled calculation of multi-physical

field, the governing equations of transfer phenomena are described as follows [26]:

Maxwell equations:

$$\vec{\nabla} \times \vec{E} = -\frac{\partial \vec{B}}{\partial t} \tag{1}$$

$$\vec{\nabla} \times \vec{H} = \vec{J} \tag{2}$$

$$\vec{\nabla} \cdot \vec{B} = 0 \tag{3}$$

$$\vec{\nabla} \cdot \vec{J} = 0 \tag{4}$$

Where, E is the electric field intensity, V/m; H represents magnetic field intensity, A/m; B is the magnetic flux density, T; J is the current density, A/m^2;
The Lorentz force is defined as follows:

$$\vec{F} = \vec{J} \times \vec{B} \tag{5}$$

The Joule heat density is expressed as:

$$Q = \frac{1}{\sigma}\vec{J} \cdot \vec{J} \tag{6}$$

The conservation equation of mass is:

$$\frac{\partial \rho}{\partial t} + \nabla \cdot (\rho \vec{V}) = 0 \tag{7}$$

The conservation equation of momentum is:

$$\frac{\partial}{\partial t}(\rho \vec{V}) + \nabla \cdot (\rho \vec{V} \times \vec{V}) = -\nabla P + \mu_{eff} \nabla^2 \vec{V} + \rho \vec{g} + \vec{F} \tag{8}$$

Where $\vec{F}$ is the Lorentz force, N/m^3. μ_{eff} is the effective viscosity, Pa · s.

The conservation equation of energy is:

$$\frac{\partial}{\partial t}(\rho H) + \nabla \cdot (\rho \vec{V} H) = \nabla \cdot (k_{\text{eff}} \nabla T) + Q \tag{9}$$

where Q is the Joule heat density, W/m^3. k_{eff} is the effective thermal conductivity, $Wm^{-1}K^{-1}$.

Determination of boundary conditions

The boundary conditions for electromagnetic field are derived from the Ampere circuital theorem [7], which is applicable to all models in this paper.

The determination of the boundary conditions for fluid flow equations is according to literatures [27], such as the no-slip condition for the solid/liquid interfaces and free-slip condition at the free surface(slag/air interface).

The boundary conditions for temperature field are determined by the experiment or calculation. Mitchell measured the temperature profile of copper mould using thermocouple [28], Fernando calculated the heat transfer coefficient of the lateral side of ingot on the basis of the heat balance [6]. In this paper, our boundary conditions are from literatures [9].

Validation of mathematical models

Model validation is a key step in model development [4]. However, it is difficult to observe the transfer phenomena directly due to the opaque molten slag and obtain precise measurements in a high temperature environment, and mathematical models are validated only by indirect methods.

At present, the general method to validate models is comparing the calculated pool profile with that of measurement [16]. However, it's hard to section large scale ingots longitudinally, and the method is not suitable for heavy ingots.

Regarding the heat transfer predictions, the temperature in slag bath and molten metal pool is measured by the thermocouple and compared with the computed results. Nevertheless, it could not be used in a close system such as the protective gas electroslag remelting.

Selected simulation examples

Numerical simulation of traditional ESR

Numerical simulation of steady state ESR process

The remelting process is unstable during the ramp-up region and subsequently maintains quasi-steady state until the ingot height reached the magnitude of the ingot diameter. In order to simplify the process of solution, the characteristic of axisymmetry is assumed for the model. The calculation domain includes the electrode, slag and ingot. Figure 2 shows the geometry model, the detailed model assumptions and boundary conditions are described in the reference [29]. The radius of electrode and mould are 0.34 m and 0.475 m respectively, the slag composition of $60\,\%CaF_2 + 20\,\%Al_2O_3 + 20\,\%CaO$ is used to remelt Cr5 steel with the 50 Hz AC power.The main results obtained with this model are presented there. The effects of melt rate on the pool profile and local solidification time (LST) are also studied for optimizing the process parameters.

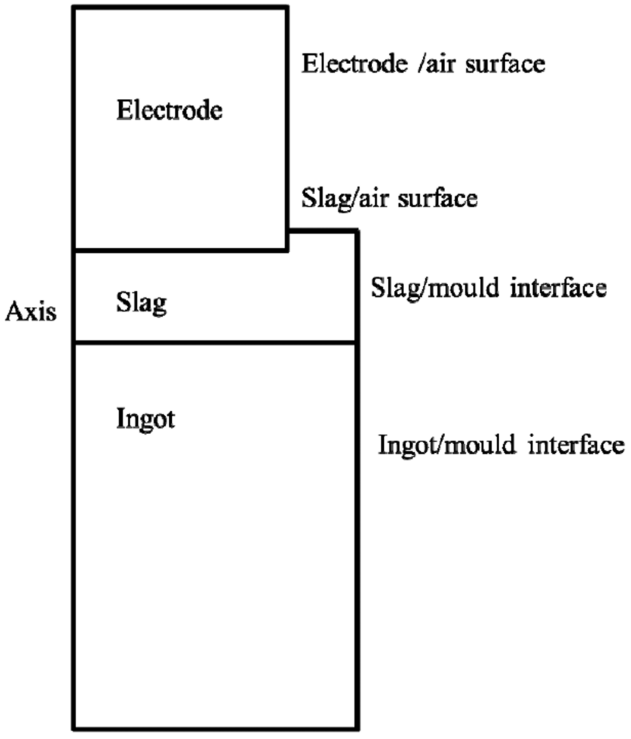

Figure 2: Sketch of the geometry model.

Figure 3 shows the electromagnetic field, velocity and temperature distribution in ESR process. The voltage drop across the slag is dominated since the electric conductivity of slag is much smaller than ingot. It is clearly seen that the current is restricted to the surface of electrode and ingot resulting from the skin effect, and the distribution of magnetic field intensity is similar with that of the current. The Lorentz force is predominated in the radial direction, towards the axisymmetry, with a maximum value at the corner of the electrode. There are two different vortexes in the slag where the maximum velocity is 0.039 m/s, the Lorentz forces drive the flow in the counter-clockwise direction under the electrode, and the clockwise vortex is driven by the buoyance near the mould wall. Figure 3(g) displays the temperature profile in the ingot and the mushy zone width. A primary analysis of ESR process is gained through the solution of model, which provides the guidance for the determination of process parameters.

Figure 4 shows the effects of melt rate on the LST, metal pool depth and maximum mushy zone width. The maximum metal pool depth and mushy zone width increase with the melt rate increasing, but the LST has a minimum at the specified melt rate. A reasonable range of melt rate could be obtained through analyzing the relationship between LST and melt rate.

The effects of parameters on steady ESR process

The steady model is employed to optimize process parameters directly linked to the ingot quality. The parametric study has been carried out with the quasi-steady state model to explore the effects of current frequency, slag height, electrode immersion depth and fill ratio on the ESR process, which provides a basis for optimizing the process parameters.

Figure 5 indicates the effect of AC current frequency on the direction of lorentz force. The direction of lorentz force is towards the axisymmetry at the slag side of the slag/pool interface for both 0.5 Hz and 60 Hz. However, the direction of lorentz force is altered for 60 Hz at the metal side of the slag/pool interface, it is horizontal and downward [30].

The metal pool becomes deeper with the slag height decreasing when the same input power is used shown in Figure 6(a) [31]. The high temperature zone of slag moves downward when the electrode immersion depth increases, which gives rise to a deeper metal pool, as shown in Figure 6(b). A shallow metal pool could be obtained by increasing the fill ratio shown in Figure 6(c), and it contributes to a uniform temperature field as well.

Numerical Simulation of transient state ESR process

The quasi-steady state model could not present the variation of physical field. Hence, it is necessary to develop a transient mathematical model including the growth of ingot, and reveals the variation of pool profile with ingot height.

Figure 7 displays the evolution of temperature distribution and pool profile. During the start-up region, a heat flow regime is imposed on the base plate resulting in a shallow pool profile. The radial heat transfer becomes gradually predominated with the ingot height increasing, and the metal pool depth increases continuously until the process reaches quasi-steady state resulting in a U-shaped pool profile. The variation of pool profile is in accordance with the experience in practice.

Numerical simulation of new ESR technology

Electroslag continuous casting technology

In order to obtain excellent solidification quality, a low melt rate is preferred in the traditional electroslag remelting process, however, it limits the production efficiency.

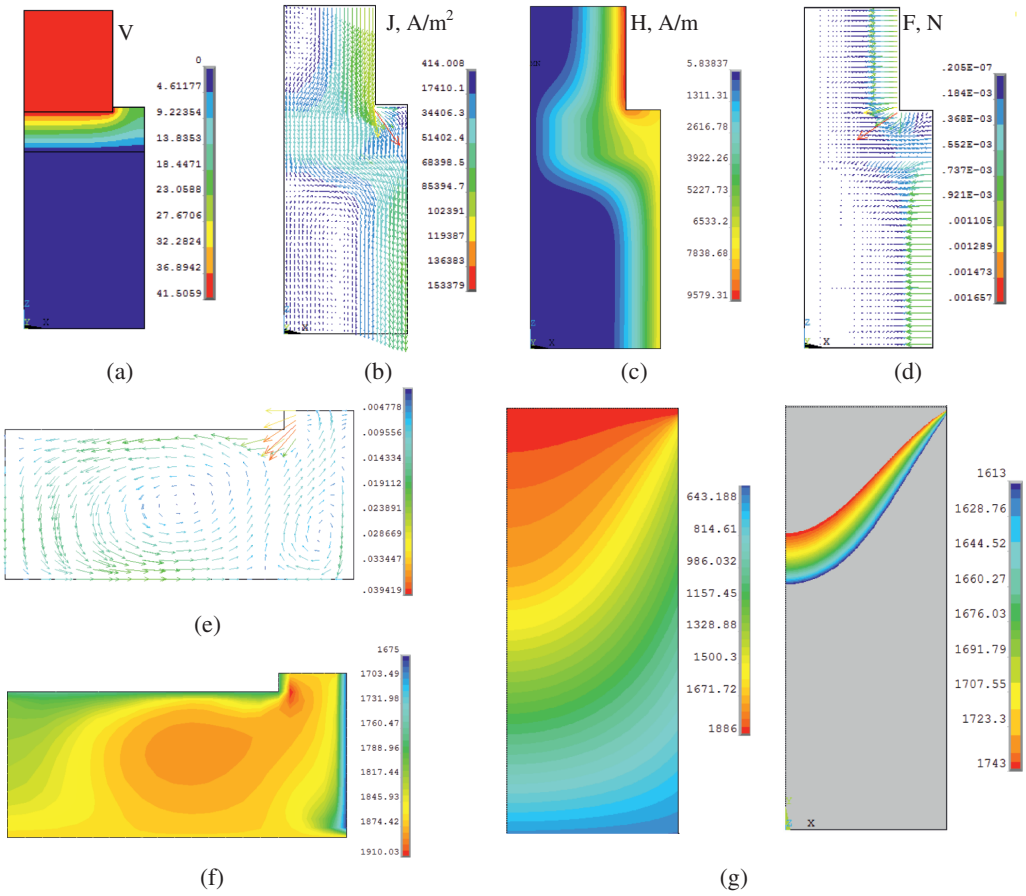

Figure 3: Field variations of electromagnetic quantities, velocity, and temperature in a steady-state ESR process. (a) Electric potential (b) Current density (c) Magnetic intensity (d) Electromagnetic force (e) Velocity distribution in slag bath (f) Temperature distribution in slag bath (g) Temperature distribution in ingot.

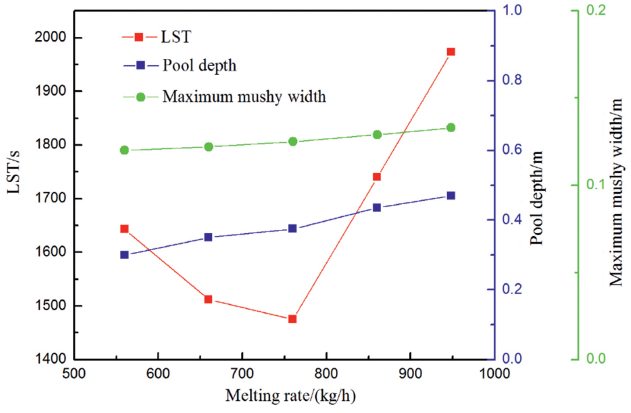

Figure 4: Relationship between melting rate and LST, metal pool depth and mushy zone width.

Therefore, electroslag continuous casting technology is developed successfully at the institute of Ferrous Metallurgy of Northeastern University combining with some new technologies such as bifilar mode, electrode changing and on-line cutting, which is characterized by high melting rate and low costs. Figure 8 shows the sketch of the electroslag continuous casting process with bifilar mode.

A 3D comprehensive mathematical model is developed to study the fluid flow and temperature distribution coupled with the electromagnetic field. The computation domain contains electrodes, slag bath and ingot, and the detailed model assumptions and boundary conditions are described in the literature [32].

A high temperature zone located between two electrodes is displayed in Figure 9, which also shows the maximum velocity at the corner of electrodes is 0.034 m/s. Since the high temperature zone is far away from the metal pool, the melt rate could be further increased compared with that of traditional ESR process. Figure 10 displays the shape of metal pool and the temperature profile in ingot.

In order to obtain better understandings of electroslag continuous casting process, the numerical

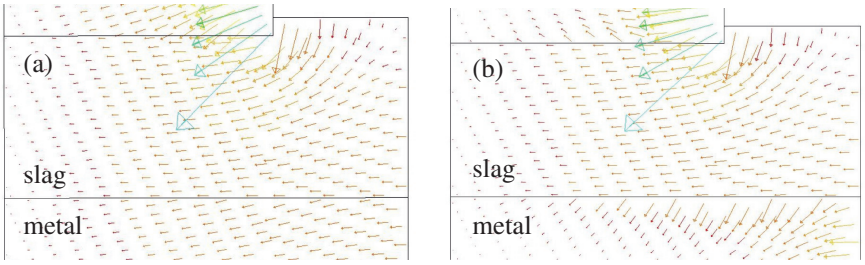

Figure 5: Influence of the AC current frequency on the direction of the Lorentz force (a) 0.5 Hz, (b) 60 Hz.

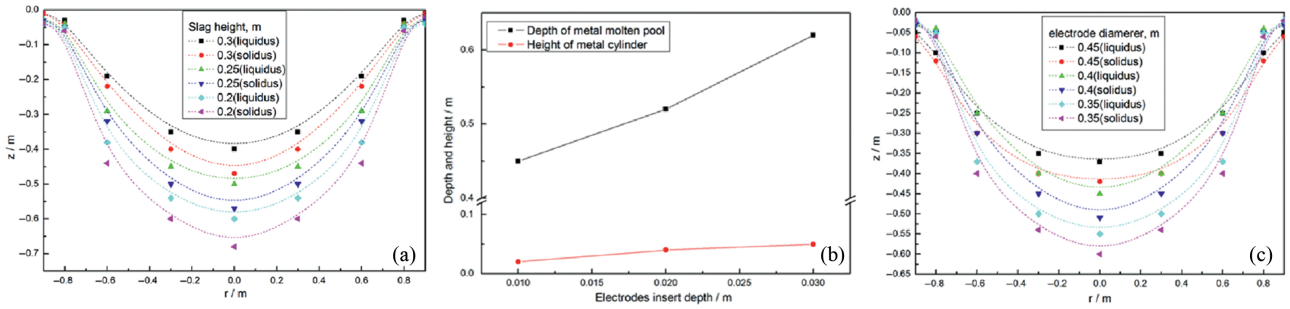

Figure 6: The effect of process parameters on the metal pool profile. (a) Slag height (b) Electrode immersion depth (c) fill ratio.

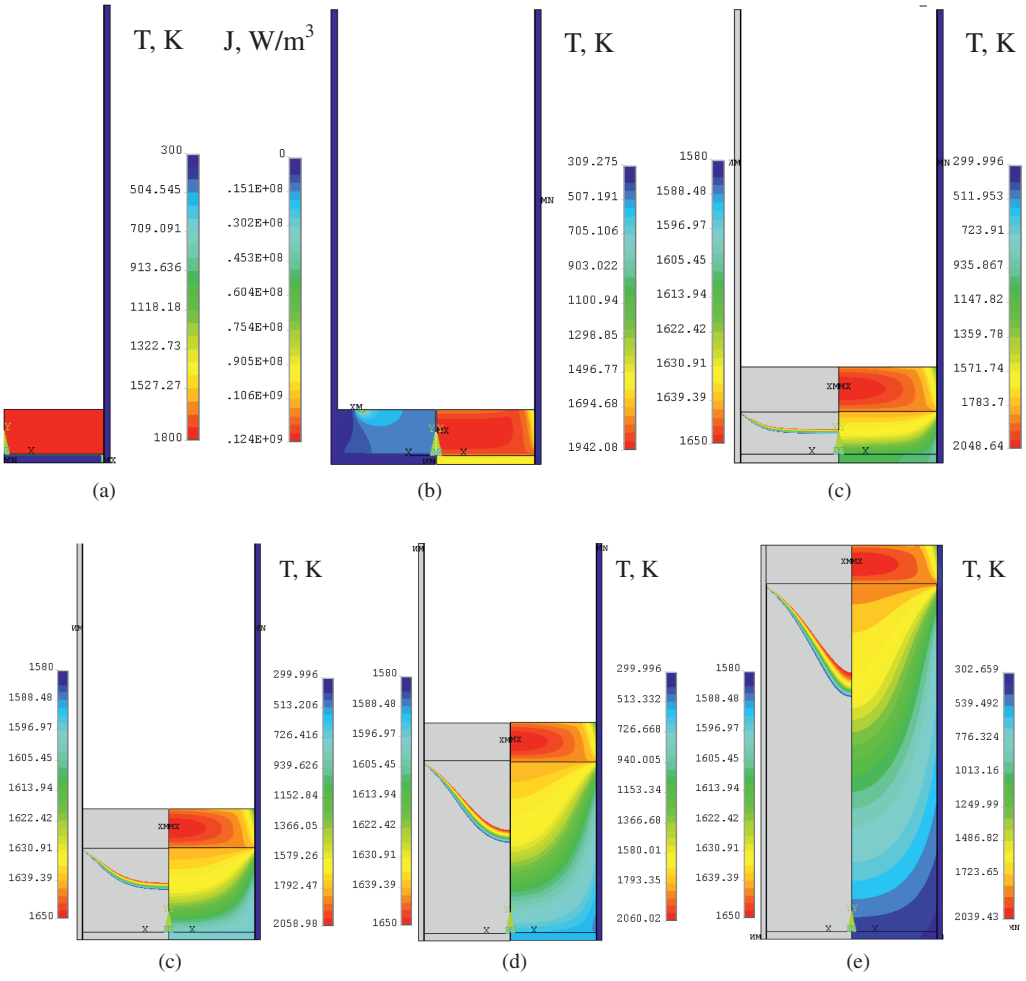

Figure 7: Evolution of temperature distribution and pool profile. (a) 1 s (b) 112 s (c) 3220 s (c) 7216 s (d) 14653 s (e) 29971 s.

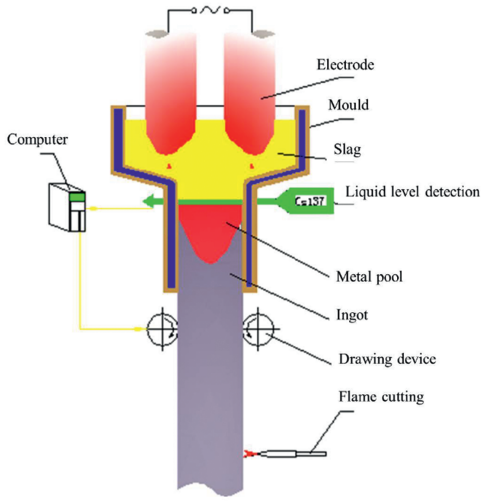

Figure 8: Sketch of the electroslag continuous casting process with bifilar mode.

simulation has been carried out. The simulation results could be used to determine the primary operation parameters which are employed to produce the W9Mo3Cr4V high speed steel successfully as shown in Figure 11(a), as seen from Figure 11(b), the billet owns a smooth surface.

Electroslag remelting large slab ingot

The large slab ingot produced by ESR is characterized by the compact structure, homogeneous composition and excellent performance. At present, The WUYANG steel company has the world's largest bifilar mode electrode ESR furnace of 50 tons. Figure 12 shows the sketch of electroslag remelting large slab ingot with bifilar mode.

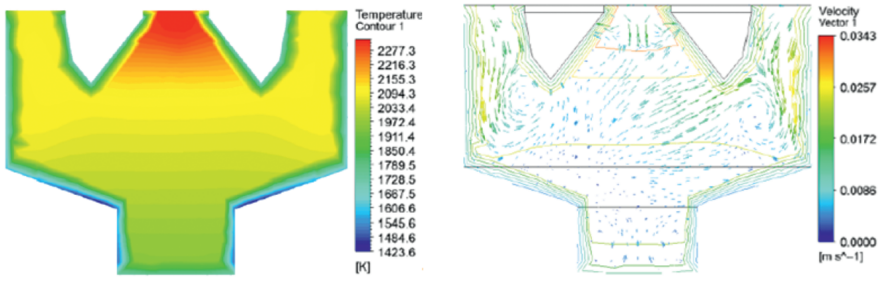

Figure 9: Temperature field and velocity distribution in slag.

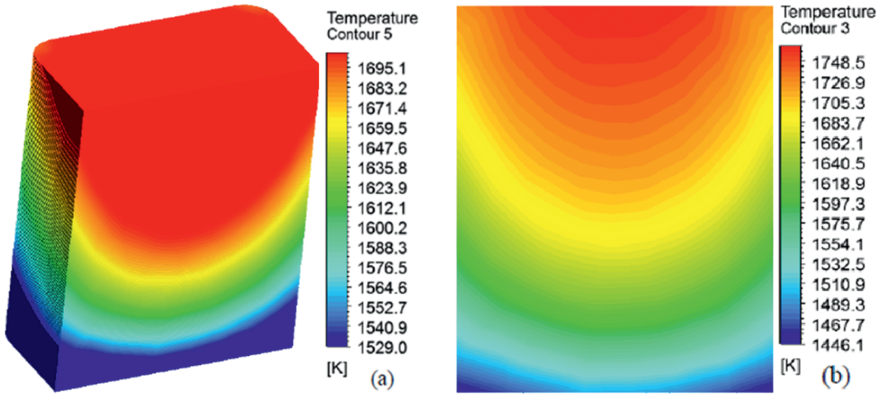

Figure 10: The shape of metal pool (a) and temperature profile of ingot (b).

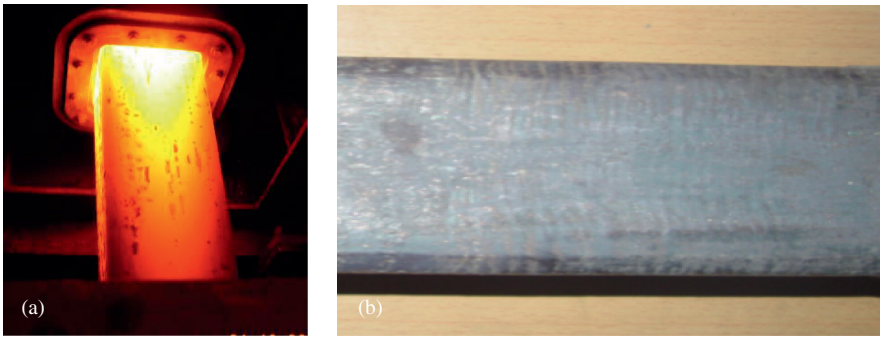

Figure 11: Electroslag continous casting billet (a) and surface quality of billet (b).

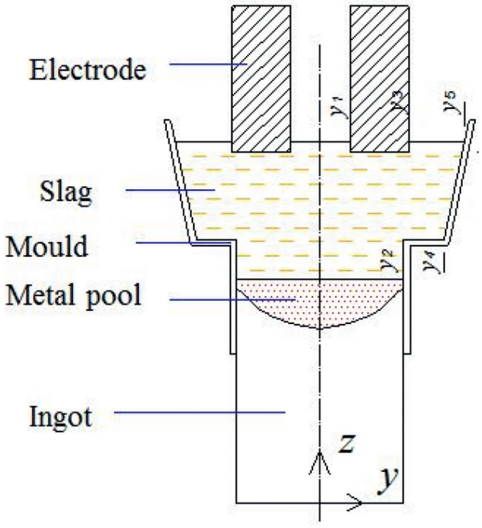

Figure 12: The sketch of electroslag remelting slab ingot.

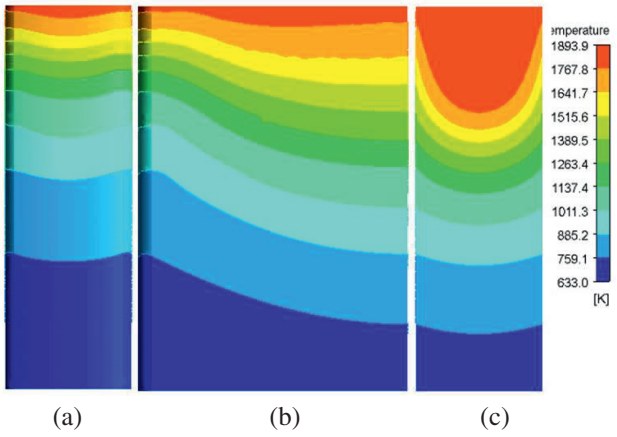

Figure 14: Temperature field distribution of slab ingot. (a) Narrow surface (b) Mid surface (c) Borad surface.

A mathematical model for electroslag remelting large slab ingot with bifilar mode is developed to investigate the electromagnetic field, fluid flow and heat transfer. The calculation domain includes the slag bath and ingot, the detailed model assumptions and boundary conditions are shown in the literature [33].

Figure 13 shows the distribution of velocity and temperature at different sections. The maximum temperature decreases gradually with the section changing from $x = 0$ m to $x = 0.6$ m, and the high temperature zone moves downward. Besides, the maximum velocity locates between two electrodes at the section of $x = 0.6$ m.

Figure 14 displays the temperature profile of ingot. The low temperature zone occurs at the corner of slab ingot with a larger cooling rate, and the center of ingot has the maximum temperature. The high temperature zone of bifilar mode electrode ESR furnace in slag locates between the electrodes, which is favorable to form a shallow pool profile and build the high grade ingot.

The common solidification defects such as double skin, ripple and macrosegregation affect the yield of ingot, which results in the increase of production costs. In order to control solidification quality of large slab ingot, the numerical simulation is carried out to optimize process parameters of electroslag remelting large slab ingot with bifilar mode, which is favorable to acquire excellent solidification quality as shown in Figure 15.

Electroslag casting with liquid metal

Electroslag casting with liquid metal (ESC LM) is an advance technology of electroslag metallurgy based on the current conducting mould(CCM) using liquid metal directly instead

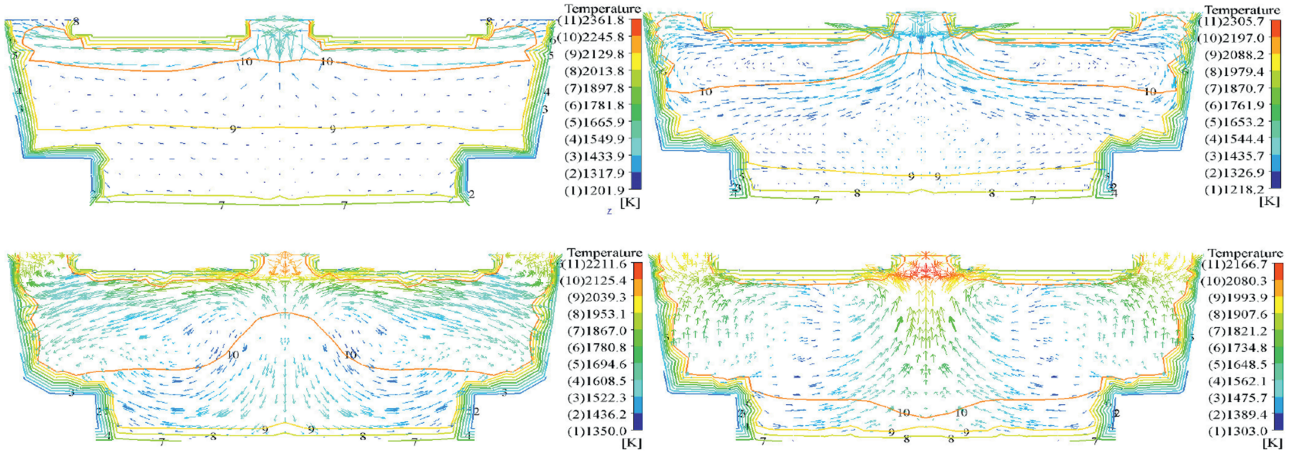

Figure 13: Temperature field and velocity field distribution of different slag sections.

Figure 15: Electroslag remelting large slab ingot with bifilar mode.

of the consumable electrode, which could reduce the production cycles and costs. ESC LM technology could be applied to manufacture composite roll, hollow or solid ingot, and so on. Figure 16 is the sketch of ESC LM for producing composite roll.

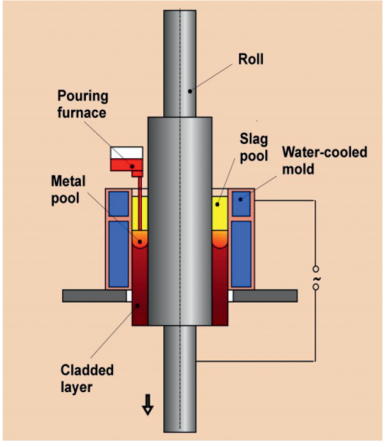

Figure 16: Sketch of ESC LM process for producing composite roll.

A steady mathematical model for the electromagnetic field, fluid flow and heat transfer has been developed to investigate the transfer phenomena in the ESC LM process. The calculation domain contains slag, roll core and composite lawyer, the required modeling equations and boundary conditions implemented in FLUENT via UDF are illustrated in the literature [34]. Besides, the effects of voltage and pouring temperature on the process are analyzed.

Figure 17 shows the distribution of current density, Joule heat, velocity and temperature in the slag bath. The maximum electric current density occurs at the bottom of current conducting mould through which the current flows, and the maximum Joule heat density also appears there. There are two different vortexes, the counter-clockwise flow occupies the bulk of slag, and the clockwise flow is driven by buoyance near the lateral wall. The high temperature zone locates at the upper slag bath, which is favorable to form a shallow metal pool and improve the quality of composite layer.

The effects of operation voltage on the temperature distribution of composite roll are shown in Figure 18. The maximum temperature in slag increases with the operation voltage, and it results in a deeper metal pool as well.

Figure 19 shows the sketch of electroslag casting hollow ingot with liquid metal. A 3D quasi-steady state mathematical model for producing hollow ingot by ESC LM has been developed to explore the fluid flow and heat transfer phenomena coupled with the electromagnetic field. The calculation domain includes slag bath and ingot, and the specific governing equations and boundary conditions are displayed in the literature [35].

Figure 20 displays the flow of slag bath, two vortexes locate at the upper of the slag, the counter-clockwise flow occupies the bulk of slag bath, and the flow tends to be clockwise near the external mould wall driven by buoyance. The maximum velocity located at the inner mould

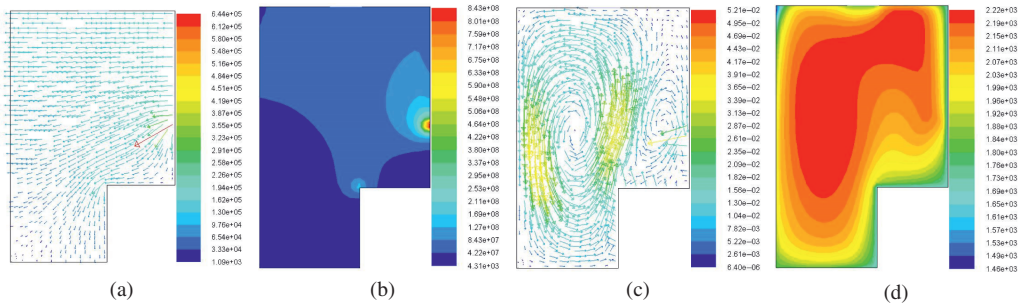

Figure 17: Distributions of parameters value of slag bath. (a) Current density, A/m^2 (b) Joule heat, W/m^3 (c) Velocity, m/s (d) Temperature, K.

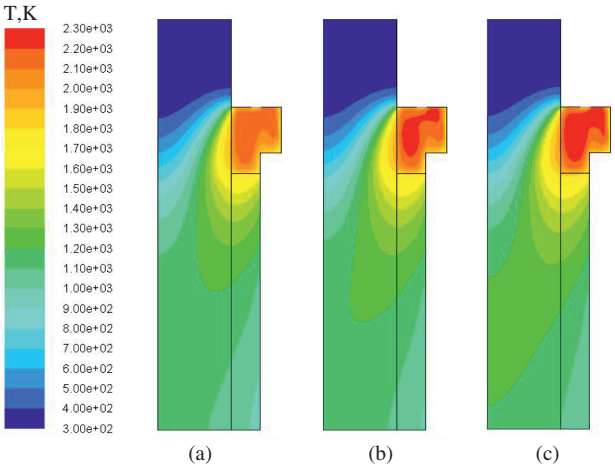

Figure 18: Temperature distributions in roll billet under different operating voltages. (a) 34 V (b) 36 V (c) 38 V.

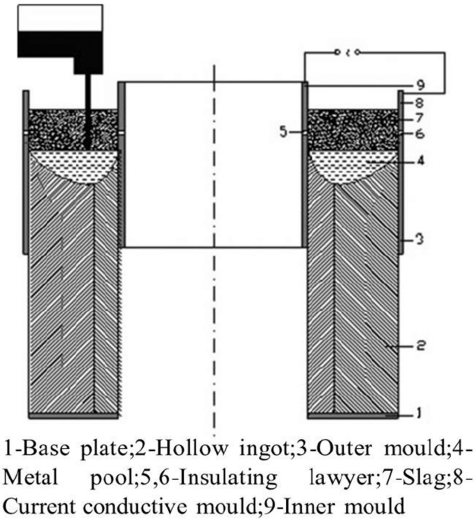

1-Base plate;2-Hollow ingot;3-Outer mould;4-Metal pool;5,6-Insulating lawyer;7-Slag;8-Current conductive mould;9-Inner mould

Figure 19: Sketch of electroslag casting with liquid metal of hollow ingot.

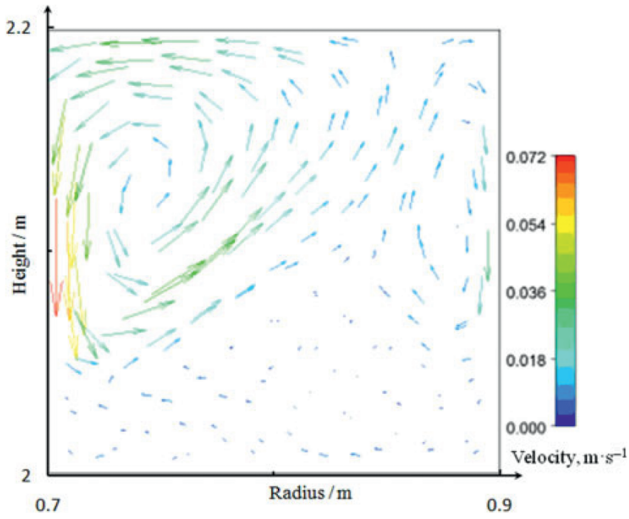

Figure 20: Velocity vectors distribution in slag pool for ESC LM hollow ingot.

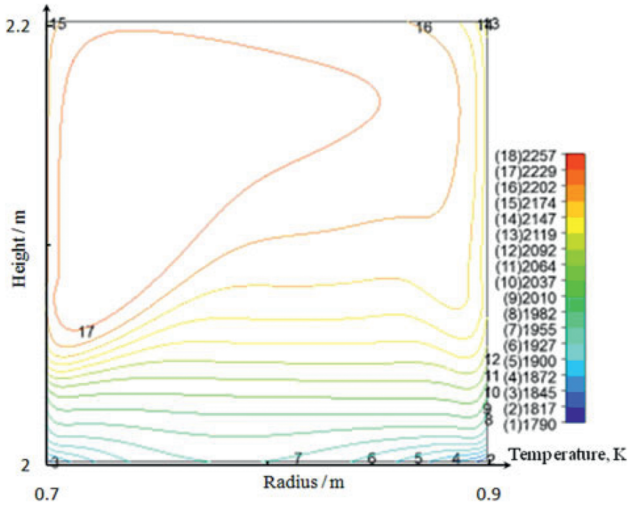

Figure 21: Temperature distribution in slag pool for ESC LM hollow ingot.

wall is 0.072 m/s. The temperature distribution in the slag bath is shown in Figure 21, the temperature distribution of upper slag bath is relatively uniform while a large temperature gradient occurs at the vicinity of slag/pool interface.

Electroslag casting with liquid metal is a new technology in the metallurgy field, and there are little published literatures about the process research and corresponding mathematical model development. The simulation results contribute to strengthen the understandings of transfer phenomena occurred in the ESC-LM process, and guide the determination of operation parameters.

Electroslag remelting hollow ingot

The solid ingot is usually applied to manufacture large cylindrical forgings with a long process, and the cracks easily take place during the process of repetitive forging and heating. Using the hollow ingot as raw materials for producing large cylindrical forgings is attractive, which could shorten process and improve forging yield. Electroslag remelting hollow ingot process provides a new method for manufacturing hollow ingot. Figure 22 shows the sketch of electroslag remelting hollow ingot.

A 3D mathematical model has been developed for electroslag remelting hollow ingot to investigate the

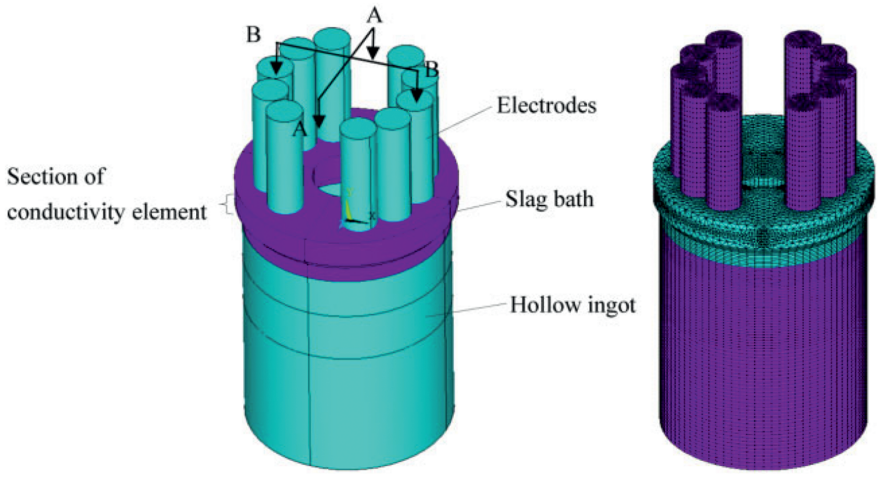

Figure 22: Sketch of electroslag remelting hollow ingot.

electromagnetic field, fluid flow and heat transfer. The calculation domain includes electrodes, slag bath and ingot, the detailed governing equations and boundary conditions are presented in the literature [36]. Besides, the effects of slag height, electrode immersion depth on the metal pool depth are also studied with the model.

Figure 23(a) shows the distribution of magnetic induction intensity. It distributes as a clock-wise loop at the surface of ingot and electrodes, and reaches its maximum at the surface of electrodes. As seen from Figure 23(b), the temperature of B-B plane is higher than that of A-A plane due to the nonuniform arrangement of electrodes. Figure 23(c) shows the temperature distribution of hollow ingot, the temperature of inner surface of mould is higher than that of external surface, which indicates that the position of the end of solidification is close to the inner mould side.

Figure 24(a) shows the effects of slag height on pool profile, the metal pool depth decreases monotonically with the increase of slag height due to more heat energy being taken away by cooling water. Figure 24(b) shows that the metal pool depth increases with the electrode immersion depth, hence a shallow electrode immersion depth is recommended to improve solidification quality of hollow ingot.

The leakage of slag and liquid steel and inner mould hold death due to solidification shrinkage are the most faced problems in the production of electroslag remelting hollow ingot, the reasonable process parameters are the key to manufacture hollow ingot successfully. The optimization parameters derived from the simulation results

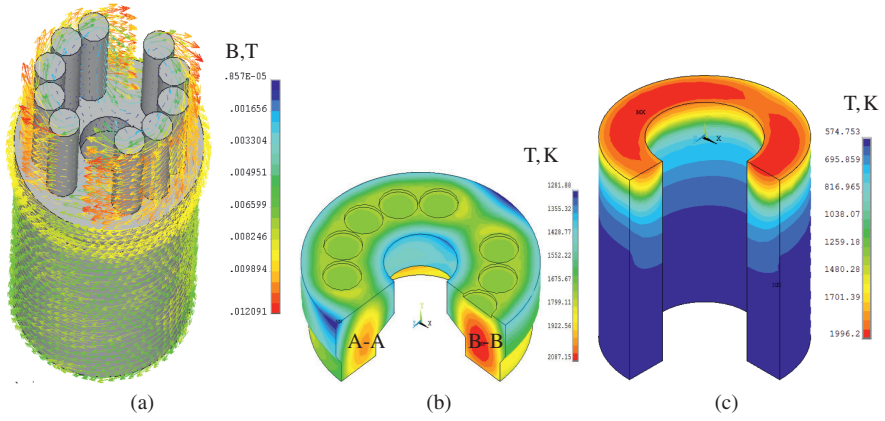

Figure 23: Distribution of parameters value in ESR, (a) Magnetic fluxdensity, (b) Temperature distribution of slag, (c) Temperature distribution of ingot.

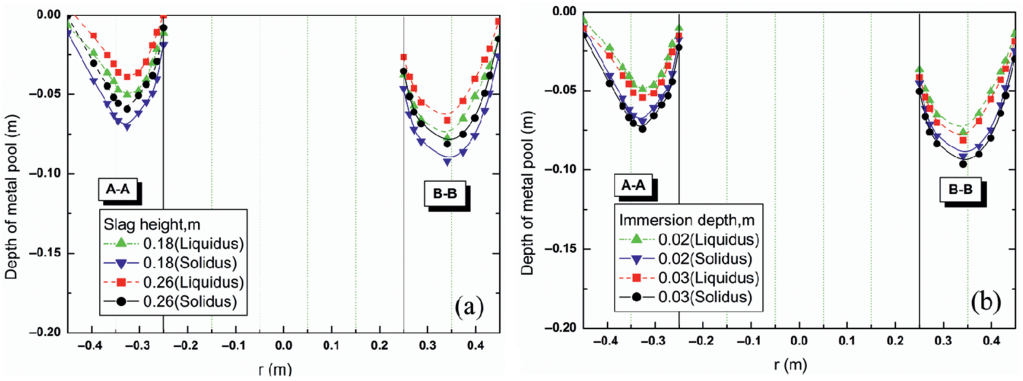

Figure 24: The effect of parameters on the molten metal pool, (a)slag height, (b) electrode immersion depth.

Figure 25: Electroslag remelting hollow ingot in plant.

are employed to produce the P91 seamless steel pipe shown in Figure 25.

Numerical Simulation of Solidification Structure

A 3D transient mathematical model of the solidification structure evolution for electroslag remelting ZG06Cr13Ni4Mo steel has been established with the coupled moving boundary and CAFE method, the pool profile from the beginning to the steady state is studied. Besides, the transition of equiaxed grains to columnar grains has been revealed [37]. The model is validated by experimental results, and it could be employed to provide a theoretical foundation for optimizing the process parameters.

Figure 26 is the evolution of solidification structure for electroslag remelting ZG06Cr13Ni4Mo steel. During the start-up region, the molten metallic droplets drop on the surface of mould bottom, a layer is rapidly and strongly chilled under the effect of cooling water shown in Figure 26(a). With the ingot growing, a large axial temperature gradient forms at the ingot bottom where the columnar grains appear, and the metal pool also becomes deeper, as shown in Figure 26(b). The latent heat releases continuously at the solidification front as solidification process proceeds, the columnar grains grow with a preferred orientation with respect to the vertical shown in Figure 26(c). The pool profile maintains invariant when the process reaches steady state, which indicates that the

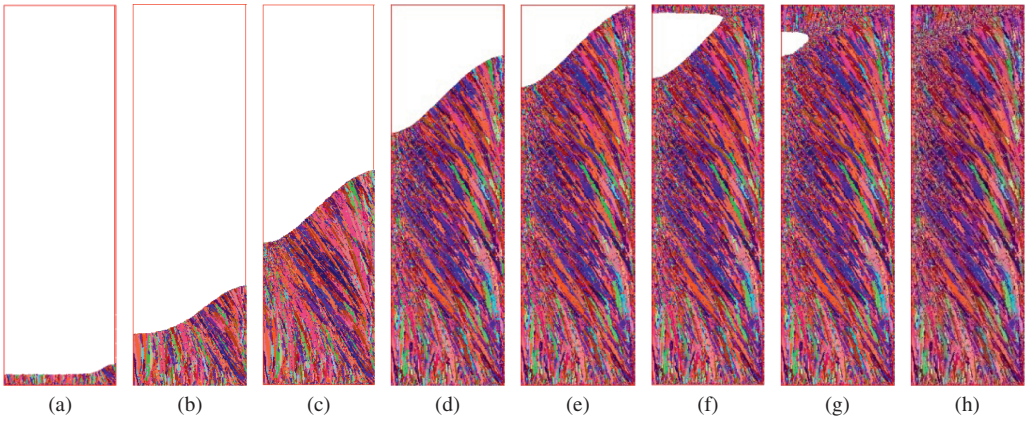

Figure 26: Solidified structure formation process in ESR of ZG06Cr13Ni4Mo ingot. (a) t = 590 s (b) t = 2,019 s (c) t = 4,038 s (d) t = 6,514 s (e) t = 8,076 s (f) t = 9,767 s (g) t = 10058 s (h) t = 10,208 s.

melt rate and solidification rate approximate balance in Figure 26(d). At the last stage, the heat flux loses its direction, the equiaxed grains begin to form within the remaining molten metal, as shown in Figure 26(e). At the end of solidification, the columnar grains grow downward from the top of the ingot due to the heat preservation effect of slag, as shown in Figure 26(f)–(h).

Figure 27 shows the comparison of solidification structure of solid ingot between the simulation and experiment [37]. The columnar grains occupy the bulk of ingot with a preferred orientation, and the fine equiaxed grain occurs at the center of ingot. The morphology of the dentrite, pool profile and the growth direction of grain agree well with the experiment.

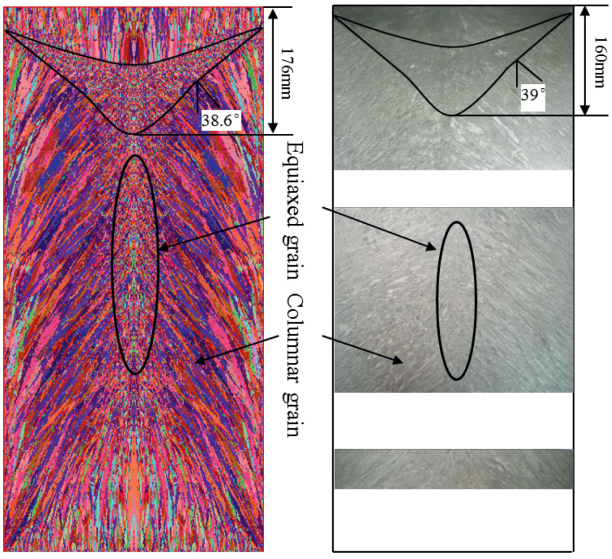

Figure 27: Comparison of solidification structure between simulation and experiment. (a) Simulation (b) Experiment.

Figure 28 shows the comparison of solidification structure of hollow ingot between the simulation and experiment [38]. The measured metal pool depth, the cylinder height, and the grain growth angle are 50.5 mm, 14 mm, and 46°, respectively, whereas the calculated results are 53 mm, 14 mm and 46°.

Figure 29 shows the effects of melt rate on the solidification structure [38]. The heat transferred to metal pool by metallic drops is dominant, and the cooling conditions sustain invariant, hence the metal pool depth and cylindrical height increase with the melt rate Besides, the growth direction of grains tends to be radial when the melt rate increases because the radial heat transfer is enhanced within a deeper metal pool.

Figure 28: Comparison of solidification structure between simulation and experiment. (a) Simulation (b) Experiment.

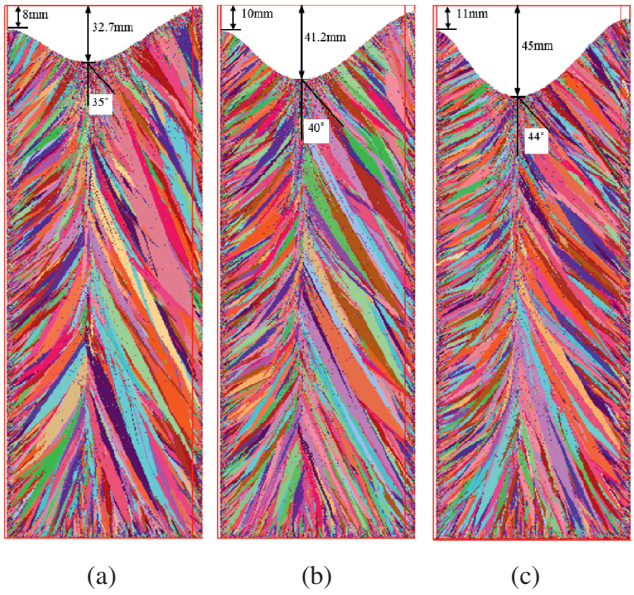

Figure 29: Solidification microstructure with different melting rate. (a) v = 0.067 mm/s (b) v = 0.083 mm/s (c) v = 0.092 mm/s

Numerical modeling of droplet formation

Firstly, A 2D steady state mathematical model of ESR is established [39], the fluid flow and heat transfer equations are solved simultaneously coupled with the

electromagnetic field which is incorporated in FLUENT via UDF. The calculation domain includes electrode, slag bath and ingot. Then, a 2D transient mathematical model coupled with VOF model which is used to trace the movement of drops is developed to predict the shape and melt rate of electrode, the calculation domain contains slag bath, air and electrode. The initial condition of the transient model is derived from the results of steady state model. Besides, the effects of voltage and interface tension on the formation and departure of droplets are also investigated.

Figure 30 shows the formation of droplet, the electrode tip melts firstly where the Joule heat reaches the maximum value, and its sharp corner gradually disappears. Two tiny droplets located at the corner of electrode moves along the surface of electrode tip to the center, and then merge into a larger droplet. As the droplet grows up to the critical size, it will depart from the electrode tip.

Figure 31(a) is the effects of voltage on droplet formation. In the same period, higher voltage gives rise to more Joule heat in the slag, hence the amount of molten liquid metal increases. The formation of droplet is also affected by the slag/metal interface tension. As the interface tension increases, the diameter of droplet is significant increased shown in Figure 31(b).

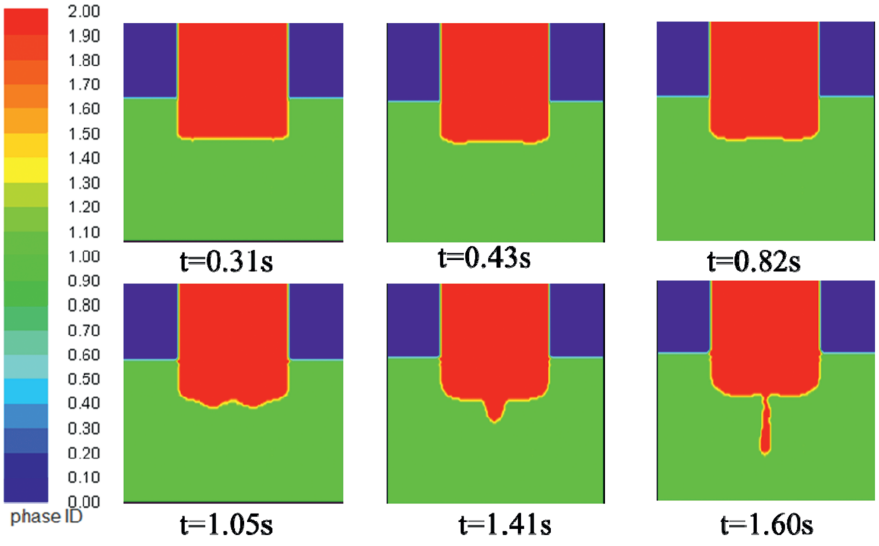

Figure 30: The process of droplet formation.

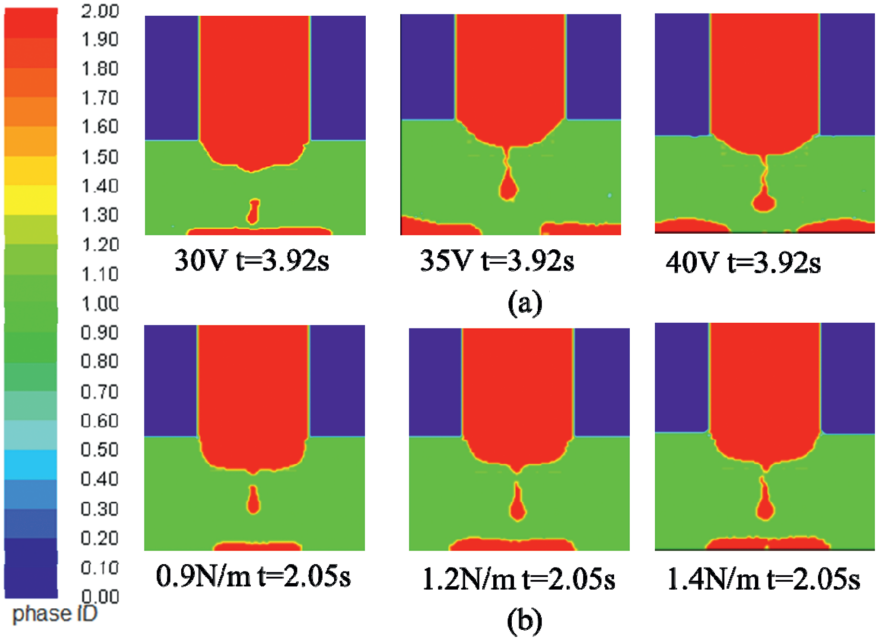

Figure 31: The droplet formation with different parameters, (a) Voltage, (b) Interface tension.

Conclusions and outlooks

Researchers have made a lot of efforts in terms of mathematical models of traditional ESR process. In order to develop a practicable model, the reasonable assumptions are necessary due to the complexity of ESR. At the beginning, the pool profile was obtained from solving the heat transfer equation without considering the flow in metal pool. Afterwards, a quasi-steady state model with the simplified assumptions was employed to investigate the coupled multi-physical field. At present, a multiphase flow model and dynamic mesh technique have been applied to investigate the transfer phenomena in ESR. The computed results agree well with the experiment, which provide effective guide for the determination of process parameters.

The new ESR technology has been developed based on the current conducting mould which brings new challenges for the numerical simulation of ESR. Researchers of special steel metallurgy laboratory at Northeastern University have made lots of efforts in terms of numerical simulation of electroslag remelting slab ingot, hollow ingot and electroslag casting with liquid metal, which is contributed to understand the transfer phenomena in the new ESR technology.

A remarkable progress of mathematical model during ESR process has been achieved by many researchers in the world. It should be further developed in following respects.

1) The coupled calculation of multi-scale model. This will need the combination of process parameters, macro-scale model(multi-phase, multi-physics field), meso-scale model(nucleation and growth of grains), micro-scale model(dendritic growth), which could be employed to optimize process parameters.
2) Simulation of the formation of air gap. The air gap was dealt with an empirical hypothesis in most literatures, a model of combining finite volume method (FVM)and finite element method(FEM) considering the solidification characteristic and mechanism of ingot should be developed to predict the formation of air gap for guiding the design of mould.
3) Pressurrized electroslag remelting(PESR) is a new technology, which is only industrialized in Germany and Austria, the simulation of PESR is not reported so far.
4) In order to avoid shrinkage cavity at the end of remelting, the current decreases progressively. The effects of hot topping operation on the quality of ingot need to be studied.
5) The model is quite sensitive to material data (eg. Thermo-physical properties of steel and slag) and process parameters (current, melt rate, and so on). It is meaningful for numerical simulation of ESR process to obtain more precise physical properties and process parameters.

It is likely that many of these domains will see significant advancement in the near future with the development of numerical simulation and the understanding of this process deepening.

Funding: This project supported by National Nature Science Foundations of China (grant No. 51434004 and U1435205). Also, this project supported by Joint Research Fund of National Nature Science Foundation of China and Baosteel Group Corporation with the grant No. U1560203. This project supported by the Fundamental Research Funds for the Central Universities (grant No N140204014).

References

[1] Y.W. Dong, Z.H. Jiang and Z.B. Li, J. Iron Steel Res.Int., 14 (2007) 7–30.
[2] X.H. Wang and Y. Li, Metall. Mater. Trans. B, 46 (2015) 1837–1849.
[3] Q. Wang, Z. He and B.K. Li, Metall. Mater. Trans. B, 45 (2014) 2425–2441.
[4] M. Hernandez and A. Mitchell, Ironmak. Steelmak., 26 (1999) 423–438.
[5] R.C. Sun and J.W. Pridegen, Metall. Mater. Trans. B, 13 (1969) 125–136.
[6] L.F. Carvajal and G.E. Geiger, Metall. Mater. Trans. B, 2 (1971) 2087–2092.
[7] A.H. Dilawari and J. Szekely, Metall. Mater. Trans. B, 8 (1977) 227–236.
[8] A.H. Dilawari and J. Szekely, Metall. Mater. Trans. B, 9 (1978) 77–87.
[9] M. Choudhary and J. Szekely, Metall. Mater. Trans. B, 11 (1980) 439–453.
[10] M. Choudhary, J. Szekely and B.I. Medovar, Metall. Mater. Trans. B, 13 (1982) 35–43.
[11] Y.M. Ferng, C.C. Chieng and C. Pan, Numer. Heat Trans. A, 16 (1989) 429–449.
[12] A. Kharicha, A. Ludwig and M. Wu, ISIJ Int., 54 (2014) 1621–1628.
[13] E. Karimi-Sibaki, A. Kharicha, J. Bohacek, M. Wu and A. Ludwing, Metall. Mater. Trans. B, 46 (2015) 2049–2061.
[14] K. Fezi, J. Yanke and M.J. Krane, Metall. Mater. Trans. B, 46 (2015) 766–779.
[15] J. Yanke, K. Fezi, R. Trice and M.J. Krane, Numer. Heat Trans. A, 67 (2015) 268–292.
[16] Q. Wang, Z. He, B.K. Li and F. Tsukihashi, Metall. Mater. Trans. B, 45 (2014) 2425–2441.

[17] Q. Wang, Z. He, G.Q. Li, C.Y. Zhu and P.J. Chen, Int. J. Heat Mass Trans., 104 (2017) 943–951.
[18] Z.H. Jiang and X.W. Jiang, J. Northeast. Univ., 54 (1988) 63–69.
[19] Z.H. Jiang and X.W. Jiang, J. Northeast. Univ., 55 (1988) 194–189.
[20] J.H. Wei and Y.L. Ren, Acta Metall. Sin., 31 (1995) 51–60.
[21] J.H. Wei and Y.L. Ren, Acta Metall. Sin., 23 (1994) 481–490.
[22] Q. Liang, X.C. Chen, H. Ren, B.S. Cheng and H.J. Guo, Adv. Mater. Res., 483 (2012) 1556–1565.
[23] V. Weber, A. Jardy and B. Dussoubs, Metall. Mater. Trans. B, 40 (2009) 271–280.
[24] Y.W. Dong, Z.H. Jiang and B.I. Medovar, Steel Res. Int., 84 (2013) 1011–1017.
[25] Y.W. Dong, Z.H. Jiang and H. Liu, ISIJ Int., 52 (2012) 2226–2234.
[26] Q. Wang and B.K. Li, ISIJ Int., 56 (2016) 282–287.
[27] K.M. Kelkar, S.V. Patankar and A. Mitchell, *Proccedings of the* 2005 *International Symposium on Liquid metal Processing and Casting*, September 18–21, 2005, Santa Fe, ASM International, USA, (2005), pp.137–144.
[28] A. Mitchell and S. Joshi, Metall. Mater. Trans. B, 4 (1973) 631–642.
[29] F.B. Liu, X. Chen, Z.H. Jiang and X. Li, J. Northeast. Univ., 35 (2014) 539–542.
[30] F.B. Liu, X.M. Zang, Z.H. Jiang, X. Geng and M. Yao, Int. J. Miner. Metall. Mater., 19 (2012) 303–311.
[31] Y.W. Dong, Z.H. Jiang, H. Liu, R. Chen and Z.W. Song, ISIJ Int., 52 (2012) 2226–2234.
[32] X.M. Zang and D. Ph Dissertation, School of Metallurgy, Northeastern University in China, (2008) 63–68.
[33] G.S. Yi and M. Dissertation, School of Metallurgy, Northeastern University in China, (2012) 45–47.
[34] Z.H. Jiang, Y.L. Cao, Y.W. Dong, D. Hou, H.B. Cao and J.X. Fan, Steel Res. Int., 87 (2016) 699–711.
[35] Y.W. Dong, Z.B. Li and Z.H. Jiang, Ironmak. Steelmak., 40 (2013) 153–158.
[36] F.B. Liu, Z.H. Jiang, H.B. Li, X. Geng, X. Chen, H. Feng and X.M. Zang, Ironmak. Steelmak., 41 (2014) 791–800.
[37] F.B. Liu, X. Chen, Z.H. Jiang, H.B. Li, X. Geng, X. Deng and X.M. Zang, Ironmak. Steelmak., 43 (2016) 385–393.
[38] X. Chen, Z.H. Jiang, F.B. Liu, J. Yu and K. Chen, Steel Res. Int., 87 (2016) 1–9.
[39] Y.W. Dong, Z.H. Jiang, J.X. Fan, Y.L. Cao, D. Hou and H.B. Cao, Metall. Mater. Trans. B., 47 (2016) 1475–1488.